




Galaxy Morphology Classification via Deep Semi-Supervised Learning with Limited Labeled Data

ZHIJIAN LUO ¹, JIANZHEN CHEN,¹ ZHU CHEN ¹, SHAOHUA ZHANG ¹, LIPING FU ^{1,2}, HUBING XIAO ¹ AND CHENGGANG SHU¹

¹*Shanghai Key Lab for Astrophysics, Shanghai Normal University, Shanghai 200234, People's Republic of China*

²*Center for Astronomy and Space Sciences, China Three Gorges University, Yichang 443000, People's Republic of China*

ABSTRACT

Galaxy morphology classification plays a crucial role in understanding the structure and evolution of the universe. With galaxy observation data growing exponentially, machine learning has become a core technology for this classification task. However, traditional machine learning methods predominantly rely on supervised learning frameworks, and their dependence on large of labeled samples limits practical applications. To address this challenge, we propose an innovative hybrid semi-supervised model, GC-SWGAN, designed to tackle galaxy morphology classification under conditions of limited labeled data. This model integrates semi-supervised generative adversarial networks (SGAN) with Wasserstein GAN with gradient penalty (WGAN-GP), establishing a multi-task learning framework. Within this framework, the discriminator and classifier are designed independently while sharing part of the architecture. By collaborating with the generator, the model significantly enhances both classification performance and sample generation capabilities, while also improving convergence and stability during training. Experimental results demonstrate that, on the Galaxy10 DECals dataset, GC-SWGAN achieves comparable or even superior classification accuracy (exceeding 75%) using only one-fifth of the labeled samples typically required by conventional fully supervised methods. Under identical labeled conditions, the model displays excellent generalization performance, attaining approximately 84% classification accuracy. Notably, in extreme scenarios where only 10% of the data is labeled, GC-SWGAN still achieves high classification accuracy (over 68%), fully demonstrating its stability and effectiveness in low-labeled data environments. Furthermore, galaxy images generated by GC-SWGAN are visually similar to real samples. Our approach provides a new solution to the challenge of needing to manually label large amounts of data in astronomy.

Keywords: Galaxies (573) — Convolutional neural networks (1938) — Ground-based astronomy (686) — Astronomy data modeling (1859) — Astronomy data analysis (1858) — Computational astronomy (293) — Astronomy data visualization (1968)

1. INTRODUCTION

The morphology of galaxies not only describes their physical appearance but also contains a wealth of important information about their growth processes, including star formation, active galactic nuclei, galaxy mergers, and gas feedback (Sandage 1986; Hashimoto et al. 1998; Lotz et al. 2006; Parry et al. 2009; Buta 2011; Rodriguez-Gomez et al. 2017). Additionally, galaxy morphology provides crucial insights into the dynamic properties of galaxies, the distribution of stellar populations, and the states of the interstellar medium (Holmberg 1958; Roberts & Haynes 1994; Deelman et al. 2004; Allen et al. 2006; Benson 2010; Conselice 2014). Therefore, understanding galaxy morphology is significant for revealing formation mechanisms, analyzing evolutionary driving factors, and comprehending the evolution of cosmic structures.

Accurate classification of galaxy morphology is a key step toward a comprehensive understanding of galaxy characteristics. With the rapid advancement of observational technologies, such as the Sloan Digital Sky Survey (SDSS) (Fukugita et al. 1996; York et al. 2000), the Legacy Survey of Space and Time (LSST) (Ivezić et al. 2019; LSST Science Collaboration: Abell et al. 2009), the Euclid Space Telescope (Laureijs et al. 2011), the Kilo-Degree Survey (KiDS) (de Jong et al. 2013), the Dark Energy Survey (DES) (Dark Energy Survey Collaboration et al. 2016; Abbott et al. 2021), the Hubble Space Telescope (HST) (Lallo & Matthew 2012), and the James Webb Space Telescope (JWST) (Gardner et al. 2009), as well as the upcoming Chinese Space Station Telescope (CSST) (Zhan 2021), we have accumulated vast amounts of galaxy image data. The scale and complexity of these data far exceed the capabilities of traditional manual classification methods, creating an urgent need to develop new automated classification technologies.

Currently, advanced algorithms, such as machine learning and deep learning, are gradually being introduced into the research of galaxy morphology classification. These methods can analyze large volumes of image data to extract potential patterns and features, enabling efficient and accurate classification. Moreover, by utilizing these automated techniques, we can significantly improve processing efficiency, conduct classifications more objectively, and reduce human biases. At the same time, continuous optimization of algorithms and the ongoing accumulation of training data are expected to further enhance classification accuracy, providing a solid foundation for our in-depth understanding of galaxy evolution.

However, existing machine learning methods for galaxy morphology classification primarily rely on supervised learning frameworks, which depend heavily on large amounts of labeled data for training. Unfortunately, labeling galaxy morphology is often time-consuming and costly, limiting the widespread application of these methods. For example, in the well-known citizen science project Galaxy Zoo, although classification has been performed on millions of galaxy images, only a few hundred thousand galaxies have been accurately classified to date (Willett et al. 2013). This labeling process not only requires substantial time and human resources but also introduces potential biases due to subjective judgments, further increasing the complexity and uncertainty of the labeling process.

Synthetic data represents an alternative method to manual annotation and shows significant potential, particularly in reducing annotation costs. However, synthetic data typically constitutes a simplified or simulated version of real data, resulting in discrepancies from the real data distribution. Consequently, any modeling or inference relying on synthetic data carries additional risks (Dagli 2023). Research indicates that models trained on synthetic data often require fine-tuning with real data prior to deployment to address these distribution discrepancies (Tremblay et al. 2018; Jordon et al. 2022).

In the absence of sufficient labeled data, constructing an accurate and efficient galaxy morphology classification model has become a significant challenge in current research. This study aims to explore a novel galaxy classification method based on semi-supervised learning. By combining a small amount of labeled data with a large volume of unlabeled data for training, this approach effectively analyzes the intrinsic structure and distribution characteristics of galaxy images, thereby improving the accuracy and generalization ability of galaxy classification.

Our model is built using semi-supervised generative adversarial networks (SGAN) (Odena 2016), integrated with Wasserstein GAN with gradient penalty (WGAN-GP) technology (Adler & Lunz 2018). This integration enhances stability and convergence during the training process while significantly improving the model’s learning capabilities. We refer to this enhanced framework as GC-SWGAN. In this study, the GC-SWGAN method will be experimentally validated on a subset of the Galaxy Zoo project—the Galaxy10 DECals dataset (Leung & Bovy 2019).

Since the release of the Galaxy10 DECals dataset, numerous studies have leveraged it to explore methods for galaxy morphology classification. These studies have employed a variety of advanced techniques from the field of deep learning, including convolutional neural networks (CNNs), residual networks (ResNets), transformers, and transfer learning, achieving significant improvements in galaxy classification accuracy (Hui et al. 2022; Maile et al. 2022; Ćiprijanović et al. 2023; Dagli 2023; Pandya et al. 2023; Yao et al. 2024). While these efforts have advanced research in galaxy morphology classification, most studies are based on a supervised learning framework, where classification performance heavily depends on the quantity of labeled data.

The Galaxy10 DECals dataset comprises approximately 17,700 galaxy samples, which is relatively small for supervised learning tasks. To enhance classification accuracy, previous studies have predominantly allocated over 80% of the dataset as training data (including test sets and validation sets), reserving less than 20% for testing purposes. Furthermore, researchers have extensively utilized various data augmentation techniques to expand the training dataset, including reflection, rotation, translation, scaling, shearing, adding Gaussian noise, and Mixup methods (Zhang 2017;

Cubuk et al. 2020). Additionally, some studies have integrated unsupervised generative adversarial networks (GANs) to generate synthetic galaxy images (Yao et al. 2024), thereby increasing the diversity of training samples.

Despite these efforts, the high dependence of supervised learning methods on labeled data significantly limits model performance. For instance, in galaxy classification tasks based on the Galaxy10 DECaLS dataset, the classification accuracy of most models has not exceeded 80% (Maile et al. 2022; Ćiprijanović et al. 2023; Huang et al. 2024; Yao et al. 2024). Only a few studies have achieved higher classification accuracy by carefully selecting data augmentation and regularization techniques or adopting complex model architectures, such as deep residual networks combined with transfer learning or hybrid transformer-convolutional architectures (Hui et al. 2022; Dagli 2023; Pandya et al. 2023). The fundamental reason for this phenomenon lies in the scarcity of labeled data, which hampers models’ ability to adequately learn the intrinsic features and distribution patterns of the data.

Our model, GC-SWGAN, offers a more flexible framework through semi-supervised learning. Unlike most previous studies, this method effectively leverages large amounts of unlabeled data for training, significantly reducing the reliance on annotated data. This approach is particularly advantageous in scenarios where annotation costs are high or where labeled data is limited, such as in the search for strong gravitational lenses (Stein et al. 2022). By employing semi-supervised learning, we not only diminish our dependence on labeled data but also enhance the model’s ability to generalize effectively across unlabeled data.

The organization of this paper is as follows: Section 2 provides an overview of the datasets utilized in this study, including the labeled Galaxy10 DECaLS dataset and the general unlabeled DECaLS images, detailing the characteristics and sources of both. Section 3 presents a comprehensive description of the data preprocessing procedures implemented for model training, which include techniques such as cropping, normalization, data augmentation, and the division into training and test datasets. Section 4 discusses the architecture design and training process of the proposed semi-supervised GC-SWGAN neural network model, emphasizing its innovative features and implementation strategies. Section 5 reports the performance evaluation of the model on the Galaxy10 DECaLS test set, comparing it with traditional supervised learning models to assess its advantages and shortcomings. Finally, Section 6 summarizes the research findings and discusses potential directions for future improvements in this study.

2. DATA

The labeled galaxy image data we use comes from the Galaxy10 DECaLS dataset, a specialized subset of the Galaxy Zoo project developed by Leung & Bovy (2019) for galaxy morphology classification. This dataset encompasses 17,736 labeled color galaxy images across the g , r , and z bands. All images in this dataset originate from the DESI Legacy Imaging Surveys, which include two DECaLS projects (Dey et al. 2019; Walmsley et al. 2022), the Beijing-Arizona Sky Survey (BASS) (Zou et al. 2019), and the Mayall z -band Legacy Survey (MzLS) (Dey et al. 2019). The galaxy morphology labels are derived from the Galaxy Zoo Data Release 2 (Lintott et al. 2008, 2011). Due to its high-quality annotations and diverse morphological representations, this dataset has been widely utilized in astronomical research.

The Galaxy10 DECaLS dataset provides a comprehensive classification of galaxy morphology, divided into 10 distinct categories. Each class, labeled from 0 to 9, corresponds to specific galaxy types: 0 - Disturbed Galaxies; 1 - Merging Galaxies; 2 - Round Smooth Galaxies; 3 - In-between Round Smooth Galaxies; 4 - Cigar Shaped Smooth Galaxies; 5 - Barred Spiral Galaxies; 6 - Unbarred Tight Spiral Galaxies; 7 - Unbarred Loose Spiral Galaxies; 8 - Edge-on Galaxies without Bulge; and 9 - Edge-on Galaxies with Bulge. This detailed classification enables precise analysis and a better understanding of galaxy morphology.

It is important to note that the Galaxy10 DECaLS dataset exhibits class imbalance, meaning that not all categories have the same number of images. For instance, the “Round Smooth Galaxies” category contains the largest number of labeled images, totaling 2,645, while the “Cigar Shaped Smooth Galaxies” category has only 334 labeled images. This imbalance may affect model training and performance evaluation, necessitating special attention in subsequent research.

Information regarding the specific number of galaxies in each category within the Galaxy10 DECaLS dataset, as well as examples of original galaxy morphology images, can be accessed via the website: <https://astronn.readthedocs.io/en/latest/galaxy10.html>. In Figure 1, we randomly display one original data sample (including galaxy images and labels) from each category in the Galaxy10 DECaLS dataset.

Our unlabeled data also originates from DECaLS (Dey et al. 2019) and shares the same underlying distribution as the Galaxy10 DECaLS images. DECaLS provides approximately two-thirds of the optical imaging coverage for the upcoming Dark Energy Spectroscopic Instrument (DESI), primarily focusing on the Northern Galactic Cap (declination

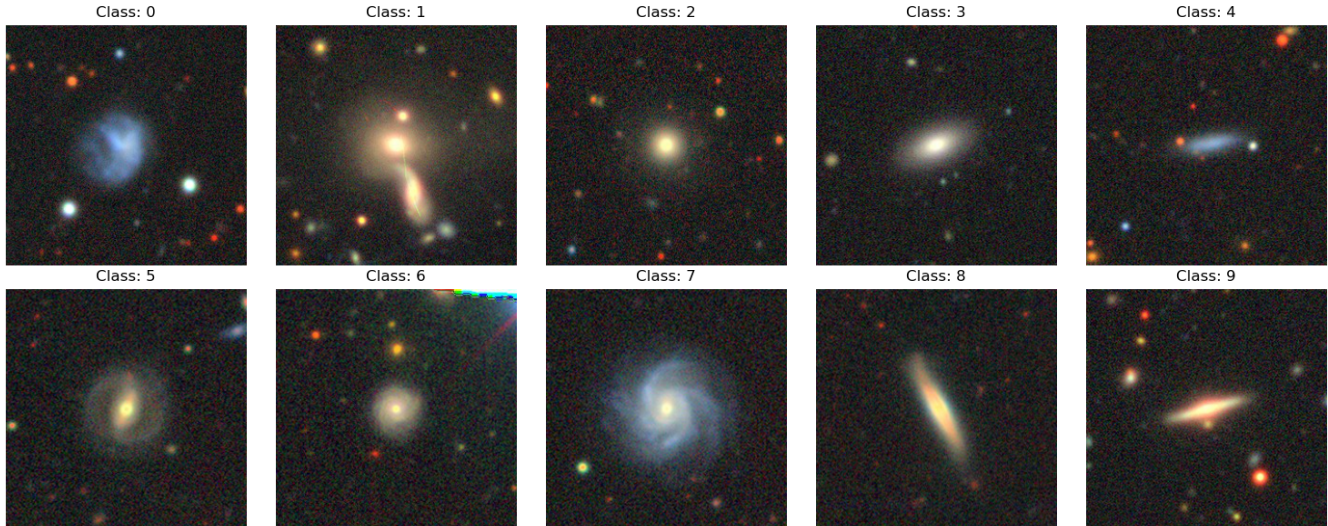


Figure 1. Random example images of each class in Galaxy10 DECals.

$\leq 32^\circ$) and the Southern Galactic Cap (declination $\leq 34^\circ$). In the observation process, DECaLS employs a sky-tiling method, conducting three independent observations with slight offsets between each, ranging from approximately 0.1° to 0.6° . The specific offsets and exposure times are adjusted based on various real-time factors to ensure uniform depth throughout the survey.

DECaLS utilizes the Dark Energy Camera (DECam) (Flaugher et al. 2015), which is installed on the four-meter Blanco telescope in Chile. The camera features a wide field of view that covers 3.2 square degrees and provides a pixel resolution of 0.262 arcseconds per pixel. The Full Width at Half Maximum (FWHM) values for the g , r , and z bands are $1.29''$, $1.18''$, and $1.11''$, respectively, resulting in an overall resolution ranging from 0.6 to 1 arcsecond. This high resolution enables DECaLS to resolve finer structures in celestial objects (DePoy et al. 2008).

Due to limitations in our computational hardware, we randomly selected approximately 18,000 color galaxy images (in the g , r , and z bands) from the Galaxy Zoo DECaLS catalog (Walmsley et al. 2022) as unlabeled samples for model training, matching the number of galaxies in the labeled Galaxy10 DECals dataset. All galaxy images were downloaded from the Legacy Survey website (<https://www.legacysurvey.org/>). These selected galaxy images represent a variety of types, ensuring that the model can learn rich morphological features from them. It is noteworthy that the Legacy Survey website contains millions of unlabeled DECaLS galaxy images, providing a vast additional data source for semi-supervised learning. The inclusion of unlabeled data enables our model to learn from a broader range of galaxy features, thus enhancing its generalization capability to unseen data.

3. DATA PREPROCESSING

To ensure data consistency and improve model performance, we conducted preprocessing on all labeled and unlabeled data. The preprocessing steps include image cropping, pixel value normalization, data augmentation, and dataset splitting. This section provides detailed explanations of these procedures.

3.1. Image Cropping

All downloaded galaxy images are 256×256 pixels, with each main galaxy centered in the image. Considering the limitations of hardware resources, we cropped the image size from 256×256 pixels to 192×192 pixels. This cropping method effectively retains the majority of the main structures of the galaxies while reducing computational resource consumption. The cropped image size remains suitable for model training, ensuring that the model can effectively learn and recognize galaxy features (Radford 2015).

3.2. Pixel Value Normalization

All pixel values in the downloaded raw images range from $[0, 255]$. We further normalize these pixel values using the following formula to convert them into the range $[-1, 1]$:

$$x^* = \frac{x - 127.5}{127.5}. \quad (1)$$

Here, x^* is the normalized pixel value, x is the original pixel value, and 127.5 is the midpoint of the range from 0 to 255. This normalization method helps accelerate model training and preserves detailed information in the images by reducing the dynamic range while maintaining contrast.

3.3. Data Augmentation

When faced with a low quantity of labeled data, selecting appropriate data augmentation strategies is crucial for enhancing classification model performance. Numerous studies have shown that data augmentation techniques significantly improve classification model performance by increasing the diversity of training data and effectively mitigating overfitting risks. However, in this study, our primary focus is on achieving accurate classification with a limited amount of labeled data by improving model architecture. Therefore, we simply employed a combination of 90-degree rotations, horizontal flips, and vertical flips as our image data augmentation approach. This choice aims to maintain the simplicity and effectiveness of the training process while allowing us to concentrate on the innovation and optimization of the model architecture.

3.4. Dataset Splitting

For the unlabeled data, we utilized approximately 18,000 DECaLS galaxy images described in Section 2 for unsupervised model training. Given the abundance of unlabeled images in the DECaLS project, this dataset has significant potential for large-scale expansion.

For the labeled Galaxy10 DECaLS dataset, we implemented several partition schemes to evaluate model performance under varying conditions of labeled data. The first scheme, Train_test_91, allocates 90% of the data for training and 10% for testing, following common practices in previous studies to assess model performance with relatively sufficient labeled data. The Train_test_73 scheme uses 70% for training and 30% for testing, further reducing the labeled training data to evaluate performance under medium-high conditions. In the Train_test_55 configuration, the dataset is split evenly, with 50% for training and 50% for testing, allowing for an assessment of the model in medium labeled data scenarios.

Moreover, the Train_test_37 scheme uses 30% for training and 70% for testing, simulating a low labeled data situation to validate the model’s robustness when labeled data is scarce. The extreme partition, Train_test_19, allocates only 10% of the data for training and 90% for testing, specifically aimed at exploring the model’s potential under conditions of very minimal labeled data. Through these partition schemes, we aim to comprehensively evaluate the model’s performance in various labeled data contexts.

4. METHODOLOGY

We have developed an improved version of the semi-supervised generative adversarial network (SGAN) (Odena 2016) by incorporating Wasserstein GAN with Gradient Penalty (WGAN-GP) (Adler & Lunz 2018) to enhance loss calculation, thereby improving the model’s stability and convergence. Additionally, we have redesigned the architecture of the discriminator D . In traditional SGAN, the discriminator D also serves as the classifier C . However, in our improved model, the discriminator and classifier are relatively independent, sharing only partial weights instead of all weights between the discriminator network D and the classifier C . This architecture is similar to a dual autoencoder (Sutskever et al. 2015) and allows certain weights to focus on the discrimination task while others specialize in the classification task, thereby enhancing the overall performance of the model. We refer to this improved model as GC-SWGAN. This section will first provide a brief overview of the design principles of SGAN, followed by a detailed description of the architecture of the GC-SWGAN neural network model. Finally, we explain the model’s training process and loss function construction.

4.1. SGAN Model

SGAN, proposed by Odena (2016), is a deep learning framework that combines Generative Adversarial Networks (GANs) with semi-supervised learning. The core idea is to enhance the model’s overall performance—both classification and generation capabilities—by simultaneously leveraging a small amount of labeled data and a large amount of unlabeled data. In many practical applications, labeled data is often scarce and expensive to obtain, while unlabeled

data is relatively abundant and easier to acquire. Consequently, SGAN has been widely applied in scenarios where labeled data is limited.

Similar to traditional GANs, SGAN primarily consists of two components: a generator G and a discriminator D . However, unlike traditional GANs, SGAN extends the conventional structure by enabling the discriminator D to not only distinguish between real and fake samples but also classify labeled samples. Specifically, the generator G generates realistic samples from random noise in an attempt to deceive the discriminator D . Meanwhile, the discriminator D undertakes two tasks: one is to differentiate between generated samples and real samples (discrimination task), and the other is to classify real samples (classification task).

In traditional GANs, the discriminator D functions solely as a binary classifier, typically outputting an estimated value to indicate whether the input image originates from the real data distribution. This is generally achieved through a feedforward neural network, with the final output being a single sigmoid unit. In contrast, the discriminator D in SGAN acts as a multi-class classifier, employing a softmax output layer that expands the output units to $N+1$, corresponding to [CLASS-1, CLASS-2, ..., CLASS-N, FAKE]. Thus, in this setup, the discriminator D not only performs the discrimination task but also serves as the classifier C .

Since the discriminator D can act as the classifier C while executing its discrimination duties, this network model is often referred to as D/C . The advantage of this design is that enhancing the performance of the discriminator D can simultaneously promote the improvement of the classifier C , and vice versa. More importantly, this mutually reinforcing relationship also enhances the performance of the generator G , thereby improving the quality of the generated samples.

Therefore, SGAN effectively integrates labeled and unlabeled data. By treating unlabeled data as real samples, the training process enhances not only the quality of the generator but also the classification performance of the discriminator, achieving synergistic optimization among G , D , and C . This optimization significantly boosts the model’s performance in both classification and generation tasks, demonstrating its substantial application potential.

4.2. Hybrid Model GC-SWGAN

The introduction of SGAN has provided a novel approach to semi-supervised learning. However, the traditional SGAN model, built upon GANs, often exhibits instability during training, which can lead to fluctuations in model performance and even mode collapse, preventing it from fully capturing the comprehensive features of the training data (Thanh-Tung & Tran 2020). To address these issues, we have enhanced SGAN by integrating Wasserstein GAN with Gradient Penalty (WGAN-GP) (Gulrajani et al. 2017; Chen 2021). By incorporating the Wasserstein distance and adopting a gradient penalty mechanism, we have significantly improved the training stability of semi-supervised learning, effectively enhancing the quality and diversity of generated images while optimizing the performance of both the discriminator and classifier.

In recent years, research has explored the application of this improved SGAN model to various computer vision tasks. For instance, Panwar et al. (2019) utilized a similar architecture to predict driver states in the field of intelligent driving, while Zeng et al. (2023) applied this model in agriculture to assess rice quality. These applications achieved good results. This paper represents the first application of such models in the field of astronomy for galaxy morphology classification, providing a new perspective and methodology for this field.

Our SWGAN-GP model architecture, as shown in Figure 2, consists of three core components: the generator G , discriminator D , and classifier C . Details of their specific structures are illustrated in Figure 3.

The generator G takes random noise z as input. First, it undergoes initial processing through a fully connected layer, Leaky ReLU activation, and a reshape layer. Subsequently, it is sequentially processed through five modules. Each module comprises a transpose convolutional layer, batch normalization, and Leaky ReLU activation to progressively reconstruct feature maps. Finally, the generator outputs the generated image through the last transpose convolutional layer with a tanh activation function as the output layer, restricting pixel values within $[-1, 1]$. This results in an output of a colored image with dimensions $192 \times 192 \times 3$.

The discriminator D and classifier C adopt a partially shared network architecture. The shared part consists of seven modules, each containing a convolutional layer, layer normalization, dropout layer, and Leaky ReLU activation to perform multi-level feature extraction on input data. The non-shared parts use fully connected layers, with an additional softmax layer added for the classifier, enabling them to achieve their respective specific tasks.

This shared mechanism not only reduces model parameters and improves computational efficiency but also allows the discriminator D to focus on distinguishing between real and generated samples, while the classifier C is able to specialize in predicting class labels of real samples.

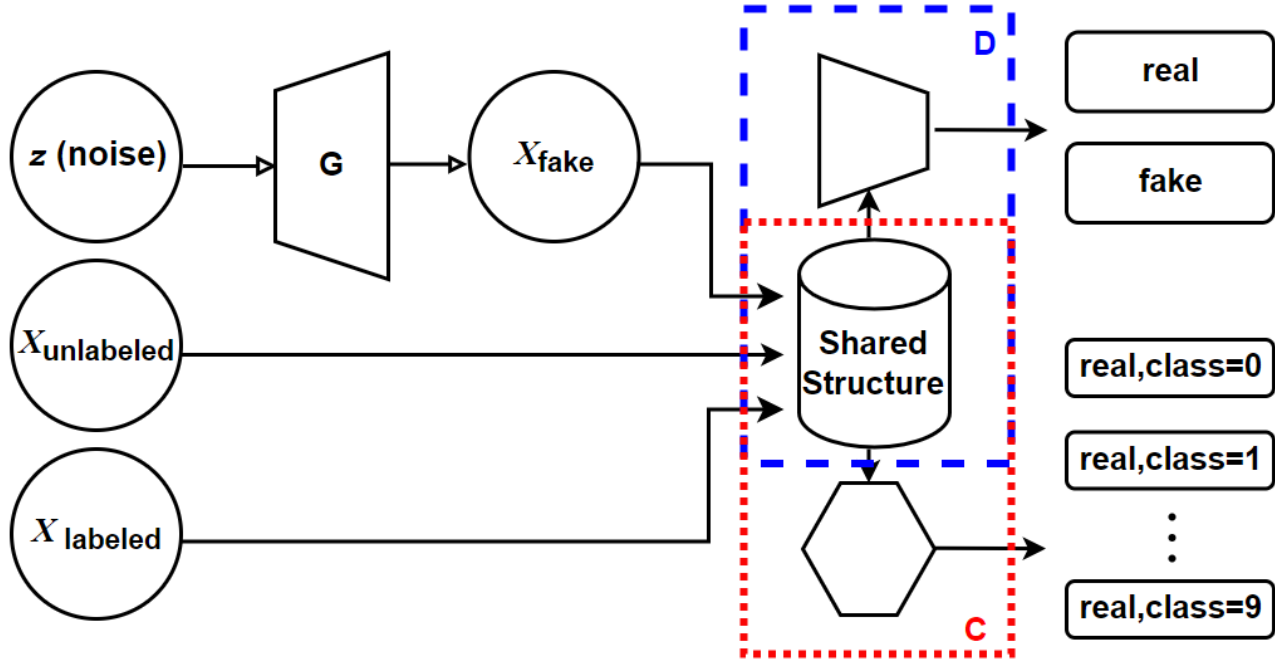


Figure 2. The network architecture of SWGAN-GP. The symbol “ z ” denotes the input random noise vector, “ $X_{unlabeled}$ ” represents the input unlabeled real images, “ $X_{labeled}$ ” indicates the input labeled real images, and “ X_{fake} ” refers to the fake images generated by the generator. G is the generator, which employs a multilayer convolutional network. D is the discriminator, whose task is to distinguish between real and fake images. C represents the classifier, which is responsible for learning to assign the correct class labels to real samples.

4.3. Model Training and Loss Function

GC-SWGAN processes data from three different sources:

1) Labeled Real Images ($X_{labeled}$): The discriminator D learns to distinguish between real and generated samples, while the classifier C learns to predict the correct class labels of the samples. The joint training of both components allows the model to simultaneously optimize feature extraction and classification performance. In this study, the Galaxy10 DECaLS dataset serves as the source of labeled real data.

2) Unlabeled Real Images ($X_{unlabeled}$): Only the discriminator D is involved in the training, optimizing its feature extraction capability by assessing the authenticity of the samples. Unlabeled DECaLS images are used as the source of unlabeled real data in this study.

3) Pseudo Images (X_{fake}): The generator G produces pseudo images by inputting random noise vectors z . The discriminator D enhances its discriminative ability by identifying these pseudo images as fake data.

While datasets 2) and 3) do not directly contribute to the training of classifier C , the shared network components between the classifier and the discriminator mean that optimizing the discriminator will simultaneously improve the classifier. This interplay creates a dynamic feedback loop in the model’s training: improvements in the performance of the discriminator D yield more accurate gradient feedback to the generator G , enabling the generation of more representative pseudo-samples. Conversely, enhancements in generator G also boost the feature extraction capabilities of discriminator D through adversarial training, indirectly optimizing the classification performance of classifier C .

This collaborative optimization mechanism allows the model to progressively enhance its data generation and classification capabilities, ultimately excelling in the task of galaxy morphology classification.

The loss function of the GC-SWGAN model consists of three components: generator loss L_G , discriminator loss L_D , and classifier loss L_C . The generator loss L_G is an adversarial loss aimed at maximizing the probability that the generated images are recognized as real by the discriminator. In the traditional SGAN, the binary cross-entropy

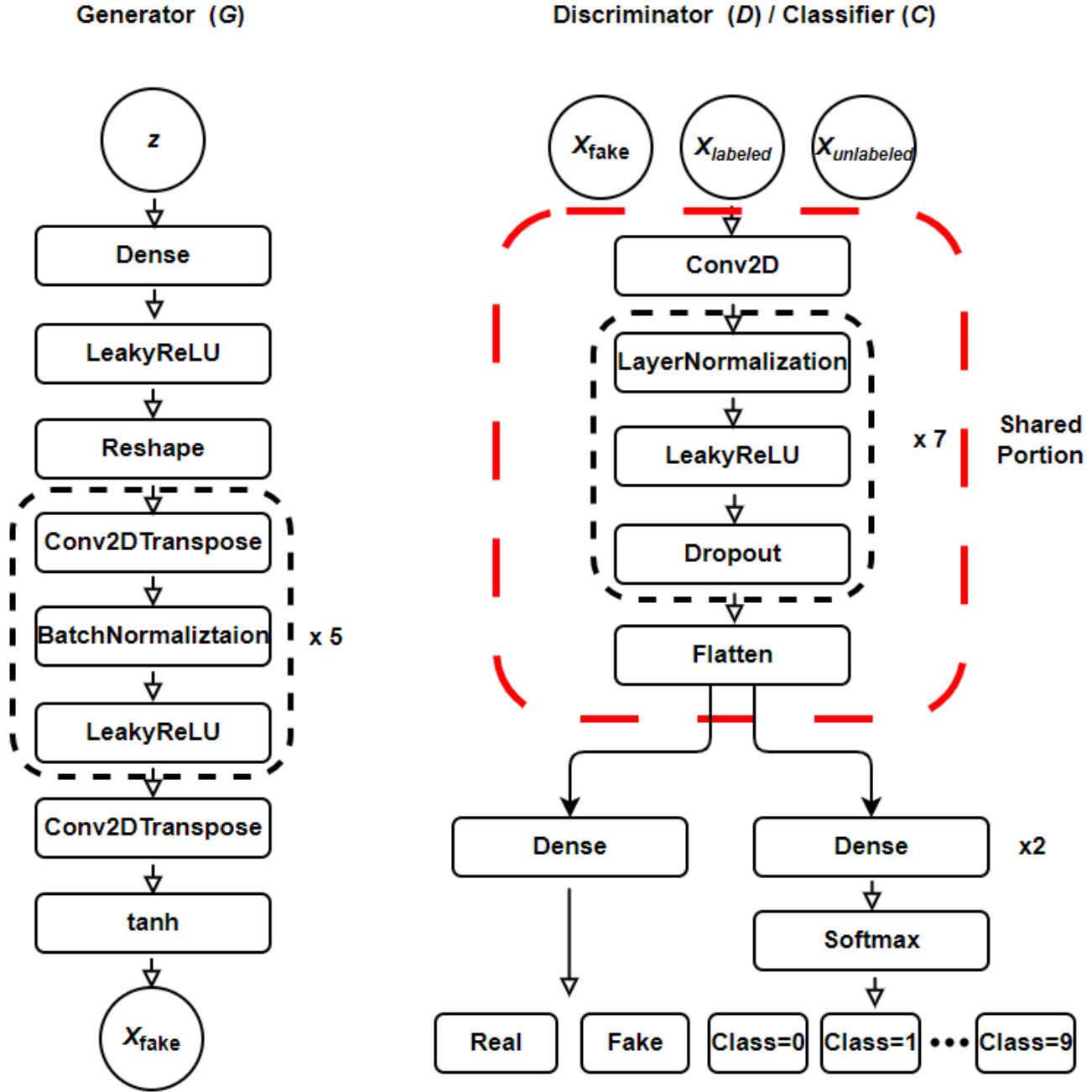


Figure 3. The detailed structures of the generator G , discriminator D , and classifier C in the SWGAN-GP model.

loss (BCE)¹ is used for this calculation. However, in our model, the generator loss is defined using the Wasserstein distance:

$$L_G = -D(G(z)), \quad (2)$$

where $G(z)$ is the output of the generator G , and $D(G(z))$ is the predicted output of the discriminator D for the generated images.

¹ https://www.tensorflow.org/api_docs/python/tf/keras/losses/BinaryCrossentropy

The loss function L_D consists of two parts. The first part uses the Wasserstein distance to measure the difference between the real samples and the generated samples:

$$L_{\text{Wasserstein}} = D(x) - D(G(z)), \quad (3)$$

where x is the real sample, and $G(z)$ is the generated sample. The second part is the gradient penalty term, which enforces Lipschitz continuity and prevents gradient explosion or vanishing. This term is defined by first creating interpolated samples x_{interp} :

$$x_{\text{interp}} = \alpha \cdot x + (1 - \alpha) \cdot G(z), \quad (4)$$

where $\alpha \in (0, 1)$ is a random number. The gradient penalty is then defined as:

$$L_{\text{GP}} = \mathbb{E} \left[\left(\|\nabla_{x_{\text{interp}}} D(x_{\text{interp}})\|_2 - 1 \right)^2 \right], \quad (5)$$

where \mathbb{E} denotes the expectation. The total discriminator loss is finally defined as:

$$L_D = L_{\text{Wasserstein}} + w_p \cdot L_{\text{GP}}, \quad (6)$$

where w_p is the weight for the gradient penalty, which is set to 10 in our study.

For the classifier loss L_C , the output of the classifier employs the softmax function to generate a probability vector, where each element corresponds to the predicted probability of a target class. This loss is calculated as a supervised loss using the categorical cross-entropy function:

$$L_C = - \sum_{i=1}^N y_i \log(p_i), \quad (7)$$

where y_i represents the true class of the input image, p_i is the predicted probability that the input image belongs to class i , and N is the total number of categories.

Through the design outlined above, we have constructed a new hybrid semi-supervised galaxy morphology classification model, GC-SWGAN. This model performs the following operations sequentially in each training iteration: First, a small batch of labeled real samples is randomly selected to train both the discriminator and the classifier. The discriminator optimizes its parameters by minimizing its loss function, which includes the Wasserstein distance and gradient penalty terms, while learning to distinguish features between real and generated samples. Simultaneously, the classifier optimizes its parameters by minimizing the classifier loss function L_C to enhance its ability to categorize real samples.

Next, a small batch of unlabeled real samples is randomly selected to further train the discriminator. In this phase, the discriminator leverages the unlabeled data to improve its ability to differentiate between real and generated samples. Finally, a small batch of random noise z is selected to generate pseudo-samples for training the generator. The generator optimizes its parameters by minimizing the generator loss function L_G , with the goal of producing more realistic samples to deceive the discriminator.

This phased training strategy enables the model to effectively leverage both labeled and unlabeled data while ensuring synergistic optimization among the generator, discriminator, and classifier. Throughout the training process, the model demonstrates high stability, effectively avoiding common issues encountered in traditional GAN training, such as mode collapse and gradient instability. In the next section, we will present the performance of this improved model in the galaxy morphology classification task, including its classification accuracy under low-annotation data conditions, the quality of the generated samples, and comparative results with other models.

5. EXPERIMENTS AND RESULTS

In this section, we will focus on evaluating the performance of the GC-SWGAN semi-supervised learning method in multi-classification tasks using the Galaxy10 DECals dataset, as well as visually assessing the quality of the images generated by the model. The model was implemented using the Keras and TensorFlow 2 libraries (Abadi et al. 2016), and all experiments were conducted on the NVIDIA L40S GPU platform. During training, the batch size was set to 64. The generator, discriminator, and classifier all utilized the ADAM optimizer (Kingma 2014), with parameters set to $\beta_1 = 0.5$ and $\beta_2 = 0.999$. The initial learning rate was set to 0.0001 and decayed exponentially after each training iteration with a decay factor of 1/1.000004. The model stopped training after 100,000 iterations, and the average training time for each experiment was approximately 20 hours.

5.1. Classification Performance

We evaluated the classification performance of GC-SWGAN using several commonly used metrics: precision, recall, and F1-score. These metrics provide insights into the model’s performance for each specific category. The corresponding definitions are as follows:

$$\text{Precision}_i = \frac{\text{TP}_i}{\text{TP}_i + \text{FP}_i}, \quad (8)$$

$$\text{Recall}_i = \frac{\text{TP}_i}{\text{TP}_i + \text{FN}_i}, \quad (9)$$

$$\text{F1-score}_i = 2 \times \frac{\text{Precision}_i \times \text{Recall}_i}{\text{Precision}_i + \text{Recall}_i}, \quad (10)$$

where, TP_i , FP_i , and FN_i represent the true positives, false positives, and false negatives for category i , respectively.

For multi-class classification tasks with balanced classes, it is standard practice to evaluate performance individually for each class and then compute an average. However, due to significant class imbalance in the Galaxy10 DECaS dataset (as discussed in Section 2), a weighted averaging approach was employed to ensure fair evaluation across all categories.

The weighted metrics are calculated using:

$$\text{Weighted Precision} = \frac{\sum_{i=0}^{N-1} (w_i \cdot \text{Precision}_i)}{\sum_{i=0}^{N-1} w_i}, \quad (11)$$

$$\text{Weighted Recall} = \frac{\sum_{i=0}^{N-1} (w_i \cdot \text{Recall}_i)}{\sum_{i=0}^{N-1} w_i}, \quad (12)$$

$$\text{Weighted F1-score} = \frac{\sum_{i=0}^{N-1} (w_i \cdot \text{F1-score}_i)}{\sum_{i=0}^{N-1} w_i}, \quad (13)$$

where w_i represents the weight assigned to each category, calculated as:

$$w_i = \frac{\text{Number of samples in class } i}{\text{Total number of samples}}. \quad (14)$$

Additionally, the overall accuracy is defined as:

$$\text{Accuracy} = \frac{\sum_{i=0}^{N-1} \text{TP}_i}{\sum_{i=0}^{N-1} (\text{TP}_i + \text{FP}_i)}, \quad (15)$$

which indicates the proportion of correctly classified instances.

We computed the evaluation metrics as mentioned above for the test sets of different data partitioning schemes defined in Section 2, and results are presented in Table 1.

Table 1. Performance metrics of the model under different data partition schemes.

Train-Test Split	Accuracy	Weighted Precision	Weighted Recall	Weighted F1-score
Train_test_91	83.60%	83.35%	83.60%	83.13%
Train_test_73	81.41%	80.96%	81.41%	80.87%
Train_test_55	80.42%	79.93%	80.42%	79.98%
Train_test_37	77.21%	77.16%	77.21%	76.63%
Train_test_28	74.68%	74.82%	74.68%	74.42%
Train_test_19	68.37%	67.85%	68.37%	67.76%

From the experimental results tabulated in Table 1, it is evident that the semi-supervised model, GC-SWGAN, exhibits remarkable classification performance across various data partitioning schemes. Notably, under a training-testing ratio where labeled data abundance is relatively high (Train_test_91), the model achieved an impressive test

set prediction accuracy of $\sim 84\%$, which surpasses the performance of many state-of-the-art classification methods currently utilized on the Galaxy10 DECals dataset.

Previous studies have consistently demonstrated the difficulty of accurately predicting galaxy morphological types using conventional multi-layer CNN networks alone on the Galaxy10 DECals dataset. For instance, Huang et al. (2024) reported achieving only approximately 32% accuracy with such approaches. This limitation has motivated the exploration of more advanced methodologies to enhance predictive performance.

Ćiprijanović et al. (2023) developed DeepAstroUDA, a universal domain adaptation technique, and applied it to galaxy classification on the Galaxy10 DECals dataset, achieving an accuracy of around 79%. Yao et al. (2024) employed GAN-based synthetic image generation to augment training data samples and evaluated three well-established deep learning architectures - AlexNet (Krizhevsky 2014), VGG (Simonyan & Zisserman 2014), and ResNet (He et al. 2016) - on the Galaxy10 DECals dataset. With a training-to-test set ratio of 9:1, these models demonstrated accuracies ranging from approximately 66% to 77%. Additionally, during their image enhancement process, they incorporate partial classification prior information as constraints and perform two types of central cropping based on galaxy type. For edge-on galaxies, the cropping size is 190×190 pixels, while for other galaxy types, it is 128×128 pixels.

While Hui et al. (2022) reported achieving approximately 89% accuracy using a pre-trained DenseNet-121 model with transfer learning and comprehensive data augmentation techniques in the Galaxy10 DECals dataset, their approach leveraged knowledge from prior models through transfer learning. Without this advantage, the model’s performance dropped to around 79%, still lower than our GC-SWGAN model’s accuracy.

It must be emphasized that the superior performance of our model can be primarily attributed to the innovative architecture design of the GC-SWGAN framework. During the training phase, we implemented only simple data augmentation techniques (e.g., 90-degree rotations, horizontal and vertical flips) without incorporating sophisticated augmentation strategies or additional regularization mechanisms. This underscores how the model’s success stems mainly from its architectural innovations rather than exhaustive optimization through extensive preprocessing.

As further evidenced by Table 1, GC-SWGAN exhibits consistent and robust performance across a range of annotation conditions: At medium-high annotation ratios (Train_test_73), the model achieves approximately 81% accuracy. Under medium annotation conditions (Train_test_55), performance remains strong at around 80%. Notably, even in more challenging low-annotation scenarios (Train_test_37), GC-SWGAN maintains a high level of classification capability with test accuracies exceeding 77%. Only under extremely limited annotation resources (Train_test_19) does performance decline significantly; however, the model still achieving commendable results with accuracy above 68%.

Figure 4 illustrates the variation in classification accuracy of the GC-SWGAN model as the proportion of labeled data used during training changes. From the figure, it can be observed that as the proportion of labeled data decreases, the model’s classification accuracy shows a gradual decline. Specifically, when the proportion of labeled data is above $\sim 20\%$, the model’s classification accuracy remains at a high level ($>75\%$), with only minor fluctuations as the labeled data proportion changes. For instance, when the proportion of labeled data decreases from 90% to 20%, the classification accuracy only drops slightly from $\sim 84\%$ to $\sim 75\%$, indicating a relatively limited change.

Importantly, it is only when the proportion of labeled data falls below $\sim 20\%$ that the model’s classification accuracy begins to decline significantly. This suggests that the GC-SWGAN model is less sensitive to the amount of labeled data, maintaining high classification performance even in scenarios where labeled data is scarce, thus demonstrating good robustness and applicability.

To further assess the model’s performance across different categories, Figure 5 presents the confusion matrix of the final trained model tested under the Train_test_91 condition on the target dataset. The values in the confusion matrix intuitively reflect the proportions of correctly classified and misclassified instances within each category. Additionally, detailed performance metrics for the model across various categories, including precision, recall, and F1-score, are listed in Table 2.

Overall, as shown in Figure 5 and Table 2, the GC-SWGAN model demonstrates satisfactory classification performance in most categories. However, there is some minor confusion between certain categories, particularly those with similar visual features, which results in a decrease in classification accuracy for those categories. Notably, the confusion between “Disturbed Galaxies” and “Non-barred Loose Spiral Galaxies” is more pronounced, which may be attributed to their asymmetric and loose structural forms. Additionally, the model faces challenges when distinguishing between specific types of spiral galaxies, including confusion among “Barred Spiral Galaxies”, “Unbarred Tight Spiral Galaxies”, and “Unbarred Loose Spiral Galaxies”. This confusion is understandable, as some features shared between these categories inherently increase the complexity of the classification task.

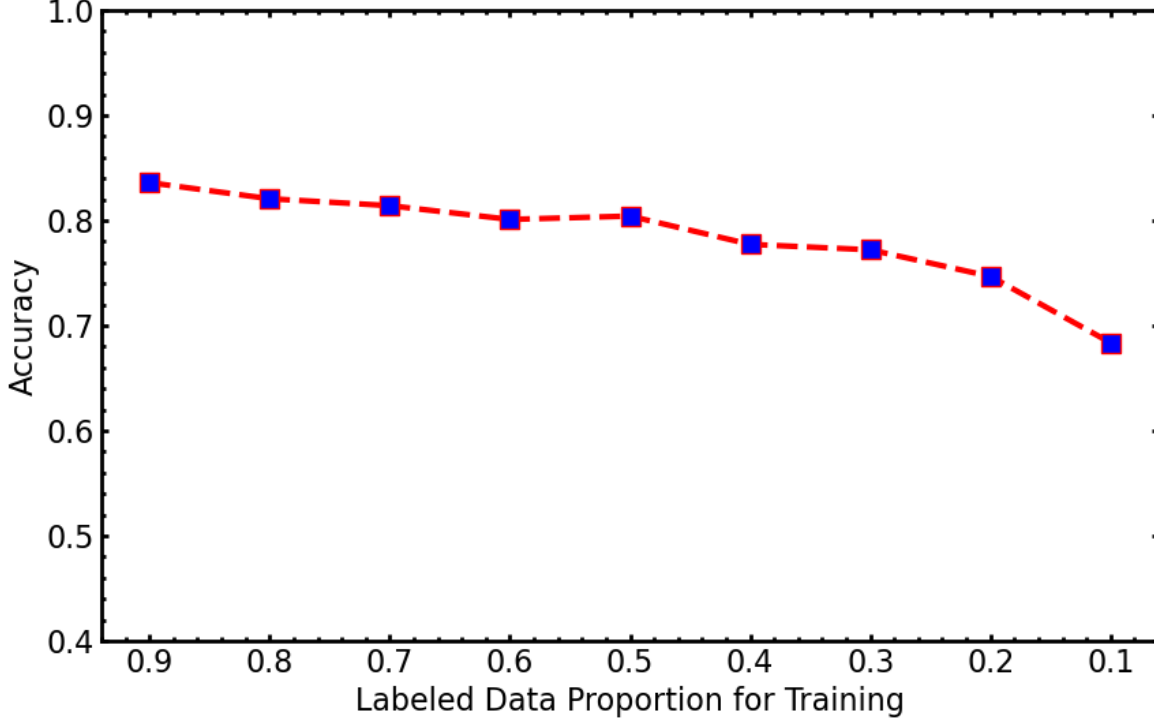


Figure 4. Variation in classification accuracy of the GC-SWGAN model with the proportion of labeled data used during training.

Table 2. Performance metrics of the model for different galaxy categories.

Galaxy Type	Precision	Recall	F1-score
Disturbed Galaxies	69.84%	43.56%	53.66%
Merging Galaxies	83.44%	80.86%	82.13%
Round Smooth Galaxies	89.86%	95.75%	92.71%
In-between Round Smooth Galaxies	82.85%	98.51%	90.00%
Cigar Shaped Smooth Galaxies	61.90%	89.66%	73.24%
Barred Spiral Galaxies	83.89%	87.19%	85.51%
Unbarred Tight Spiral Galaxies	77.14%	72.19%	74.59%
Unbarred Loose Spiral Galaxies	78.04%	73.16%	75.52%
Edge-on Galaxies without Bulge	89.88%	92.64%	91.24%
Edge-on Galaxies with Bulge	92.55%	88.32%	90.39%

5.2. Application of Classifiers on Unlabeled DECaLS Data

The well-trained GC-SWGAN classifier can be directly applied to the unlabeled DECaLS dataset for type prediction. Although the lack of type labels prevents direct quantitative comparison, we conducted a visual assessment of several unlabeled DECaLS images to validate the model’s applicability to such datasets. Figure 6 presents examples of the classifications made by the GC-SWGAN classifier on these unlabeled galaxy images, with each category showcasing a representative image.

As can be seen from the figure, the model demonstrates excellent performance on the new data, further proving its strong generalization capability. However, it should be noted that due to the higher diversity of galaxy morphologies in the unlabeled DECaLS images, our model can only be used for preliminary classification of this dataset. To

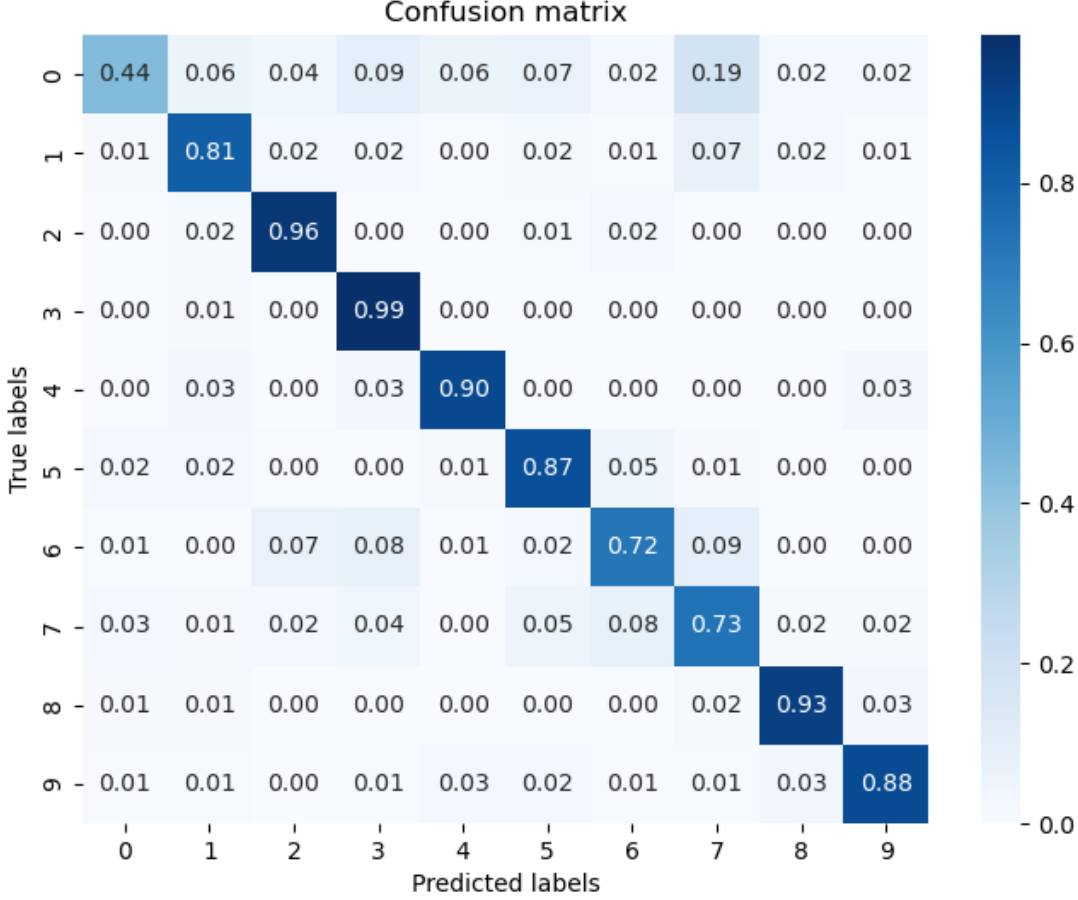


Figure 5. Confusion matrix for the target test set, illustrating confusion among morphologically similar classes.

ensure the accuracy of the classification results, a detailed manual review and inspection of the results will still be necessary to address any potential omissions or misclassifications by the model. Furthermore, future work could consider incorporating more diverse training data or fine-tuning the model to further enhance classification accuracy and robustness.

Additionally, Table 2 reveals that the model excels in most predefined categories. Taking “Round Smooth Galaxies” as an example, the model achieves classification precision, recall, and F1-scores of 89.86%, 95.75%, and 92.71%, respectively, for this category. For “Merging Galaxies”, the model’s classification precision, recall, and F1-scores also reach 83.44%, 80.86%, and 82.13%, respectively. These results indicate that GC-SWGAN can be effectively applied to unlabeled DECaLS samples to assist in screening specific types of galaxies. Figure 7 presents examples of “Merging Galaxies” selected by this classifier, showcasing diverse morphological features such as irregular bridges, tidal tails, and varying degrees of asymmetry. Future research could further analyze these selected galaxy samples to explore the underlying physical mechanisms and evolutionary histories.

5.3. Visual Analysis of Generated Images

In our GC-SWGAN model, a collaborative optimization mechanism exists among the generator G , discriminator D , and classifier C . Through this mechanism, the model achieves significant improvements in both classification performance and image generation quality. Specifically, the generator learns more comprehensive feature representations from feedback provided by the discriminator and classifier, enabling it to produce higher-quality samples.

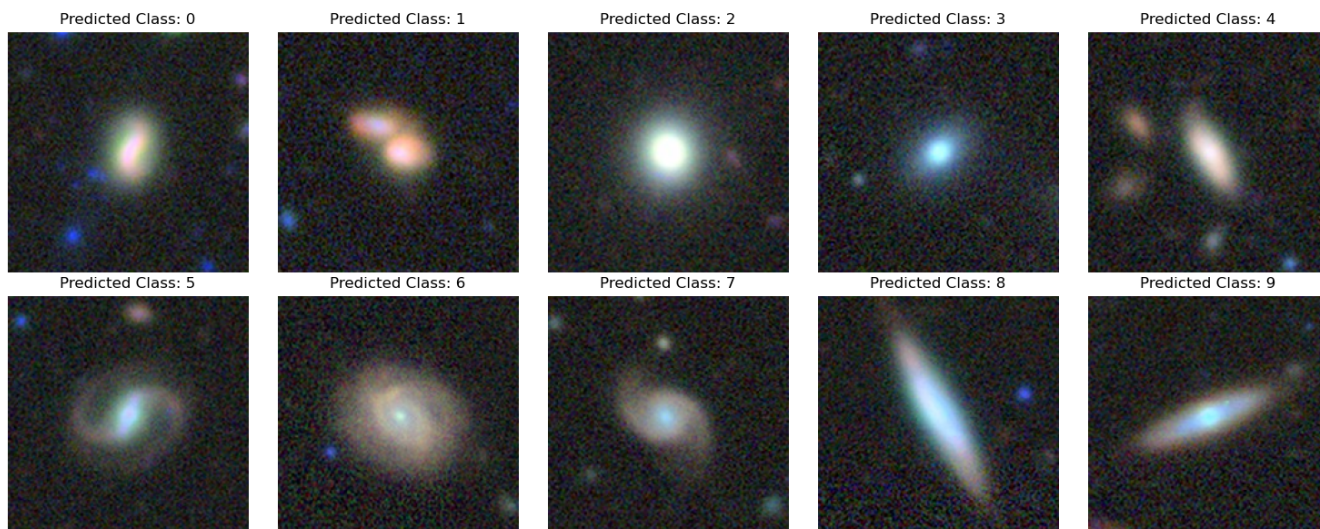


Figure 6. Random example images of each class in unlabeled DECaLS dataset.



Figure 7. Some example images of Merging Galaxies in unlabeled DECaLS dataset.

While evaluating the quality of generated images is not the primary focus of this study, we conducted a simple visual inspection to assess their realism. Figure 8 shows randomly selected samples from each category produced by the generator, including fake galaxy images with predicted labels. These examples demonstrate that images generated using the GC-SWGAN method are visually highly similar to real galaxies.

The generated samples exhibit remarkable diversity in morphological types, such as spiral galaxies, elliptical galaxies, and irregular galaxies. In terms of detailed features, the generated galaxy images closely resemble real galaxies in terms of morphology, brightness, and structure. Notable features like spiral arms, galactic nuclei, and dust lanes are effectively captured. Based on this visual analysis, the generated samples are nearly indistinguishable from real galaxies, further validating the generator’s high-quality generation capability. This advanced generation ability also enhances the discriminator’s feature extraction capabilities through adversarial training, thereby optimizing the classifier’s classification performance.

Furthermore, by expanding the dataset for model training with these high-quality images generated by the generator, we can enhance the model’s ability to identify galaxy morphologies with extremely high diversity and improve its

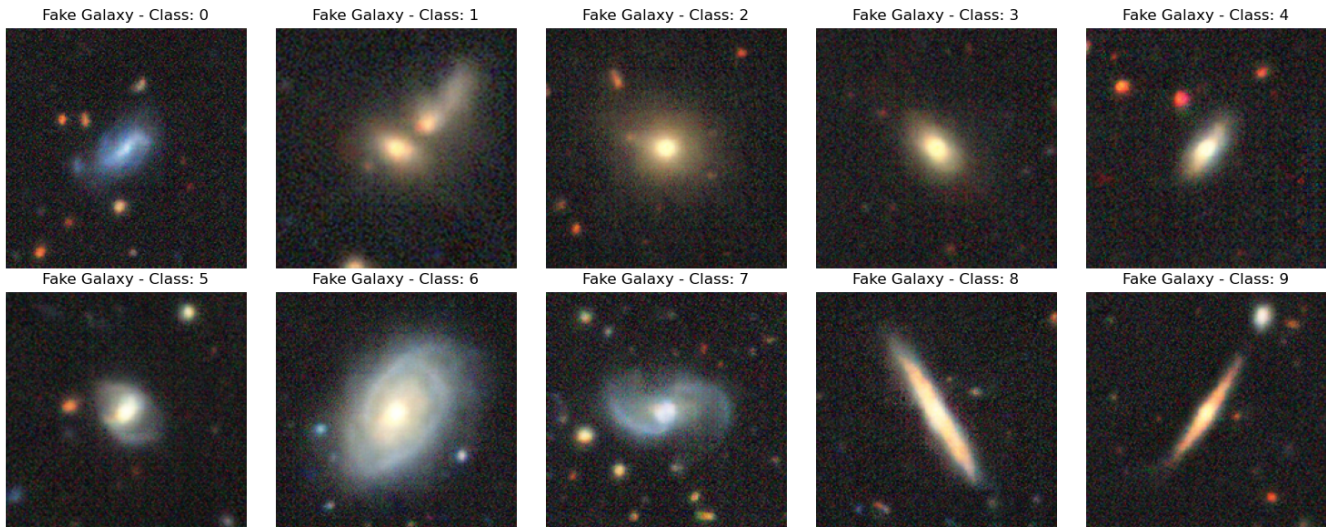


Figure 8. Randomly selected samples from each category in the generated fake galaxies produced by the generator.

robustness. This method exhibits promising potential, and we believe it is a direction worth further in-depth research and exploration.

6. SUMMARY

We propose a new hybrid semi-supervised model, GC-SWGAN, to address the challenge of galaxy morphology classification under conditions of limited labeled data. This model is trained by combining a small labeled dataset with a large collection of unlabeled data, resulting in significant improvements in classification performance. Our model is based on the traditional SGAN architecture and is optimized by incorporating Wasserstein GAN along with its improved version, WGAN-GP (Wasserstein GAN with Gradient Penalty).

By introducing Wasserstein distance and gradient penalty mechanisms, we significantly enhance the training stability of the semi-supervised learning process while improving the quality and diversity of generated images. Additionally, we optimize the designs of the discriminator and classifier by employing a method that allows for their independent architecture while sharing some components of the network. Through the collaborative optimization of the discriminator, generator, and classifier, the model’s classification performance and generative capability have been significantly enhanced.

The results of our experiments on the Galaxy10 DECaLS dataset demonstrate that GC-SWGAN excels in the galaxy classification task. When sufficient labeled data is available (e.g., using 90% of the data for training), the overall classification accuracy reaches approximately 84%, surpassing most existing supervised learning methods. Furthermore, even with limited labeled data, GC-SWGAN maintains strong performance, achieving results comparable to many supervised methods with only one-fifth of the labeled data. In situations with very scarce labeled data (e.g., using only 10% of the labeled data), the model still achieves high classification accuracy. Analysis of the confusion matrix and detailed performance metrics across various categories further indicates that the model performs well in most categories, with confusion occurring primarily between visually similar categories. This demonstrates its effectiveness in feature extraction and category differentiation.

The well-trained GC-SWGAN classifier can be directly applied to the unlabeled DECaLS dataset for preliminary type predictions. Our results show that the model performs excellently on new data and can effectively assist in identifying specific types of galaxies, fully demonstrating its strong generalization capability. Future research could further analyze the selected samples to explore the underlying physical mechanisms and evolutionary processes, thereby enhancing our understanding of galaxy morphology and evolution.

In addition, the GC-SWGAN model also exhibits high quality in generating galaxy images, with the generated galaxy samples showing high consistency with real galaxies in terms of morphology, brightness, and structure, as well as demonstrating rich diversity. This result indicates that the GC-SWGAN, after multiple iterations of training, can generate high-quality synthetic samples.

However, despite the impressive performance of the GC-SWGAN model, there is still potential for further enhancement. Due to computational resource limitations, the amount of unlabeled data used during training is currently equal to that of the labeled data. Future research could explore incorporating larger quantities of unlabeled image data to facilitate better learning of the intrinsic structures and distribution characteristics of the images, thus improving classification accuracy and generalization ability. Additionally, employing more data augmentation techniques, such as Mixup (Zhang 2017) and RandAugment (Cubuk et al. 2020), could help expand the labeled dataset and enhance the model’s robustness and effectiveness. Furthermore, implementing advanced input image preprocessing techniques, such as morphological opening operations (Hui et al. 2022) and increasing the resolution of input images (Luo et al. 2024), could enable the model to extract features more effectively and fully leverage its potential.

7. ACKNOWLEDGMENTS

Z.J.L. acknowledges the support from the Shanghai Science and Technology Foundation Fund (Grant No. 20070502400) and the scientific research grants from the China Manned Space Project. S.H.Z. acknowledges support from the National Natural Science Foundation of China (Grant No. 12173026), the National Key Research and Development Program of China (Grant No. 2022YFC2807303), the Shanghai Science and Technology Fund (Grant No. 23010503900), the Program for Professor of Special Appointment (Eastern Scholar) at Shanghai Institutions of Higher Learning, and the Shuguang Program (23SG39) of the Shanghai Education Development Foundation and Shanghai Municipal Education Commission. L.P.F. acknowledges the support from the National Natural Science Foundation of China (NSFC 11933002). H.B.X. acknowledges the support from the National Natural Science Foundation of China (NSFC 12203034) and the Shanghai Science and Technology Fund (22YF1431500). This work is also supported by the National Natural Science Foundation of China under Grant No. 12141302.

The DESI Legacy Imaging Surveys consist of three individual projects: the Dark Energy Camera Legacy Survey (DECaLS), the Beijing-Arizona Sky Survey (BASS), and the Mayall z-band Legacy Survey (MzLS). These surveys utilized facilities such as the Blanco, Bok, and Mayall telescopes, supported by the National Science Foundation (NSF) and operated by different observatories including NSF’s NOIRLab.

We thank the respective teams and funding agencies for making these data publicly available. For detailed acknowledgments and funding information, please refer to the original publications and data release notes.

REFERENCES

- Abadi, M., Barham, P., Chen, J., et al. 2016, in 12th USENIX symposium on operating systems design and implementation (OSDI 16), 265–283
- Abbott, T. M. C., Adamów, M., Aguena, M., et al. 2021, *ApJS*, 255, 20, doi: [10.3847/1538-4365/ac00b3](https://doi.org/10.3847/1538-4365/ac00b3)
- Adler, J., & Lunz, S. 2018, *Advances in neural information processing systems*, 31
- Allen, P. D., Driver, S. P., Graham, A. W., et al. 2006, *Monthly Notices of the Royal Astronomical Society*, 371, 2
- Benson, A. J. 2010, *Physics Reports*, 495, 33
- Buta, R. J. 2011, arXiv preprint arXiv:1102.0550
- Chen, H. 2021, *Journal of Physics: Conference Series*, 1827, 012066
- Ćiprijanović, A., Lewis, A., Pedro, K., et al. 2023, *Machine Learning: Science and Technology*, 4, 025013
- Conselice, C. J. 2014, *Annual Review of Astronomy and Astrophysics*, 52, 291
- Cubuk, E. D., Zoph, B., Shlens, J., & Le, Q. V. 2020, in *Proceedings of the IEEE/CVF conference on computer vision and pattern recognition workshops*, 702–703
- Dagli, R. 2023, arXiv preprint arXiv:2304.05350
- Dark Energy Survey Collaboration, Abbott, T., Abdalla, F. B., et al. 2016, *MNRAS*, 460, 1270, doi: [10.1093/mnras/stw641](https://doi.org/10.1093/mnras/stw641)
- de Jong, J. T., Verdoes Kleijn, G. A., Kuijken, K. H., et al. 2013, *Experimental Astronomy*, 35, 25
- Deelman, E., Blythe, J., Gil, Y., et al. 2004, in *Grid Computing: Second European AcrossGrids Conference, AxGrids 2004, Nicosia, Cyprus, January 28-30, 2004. Revised Papers*, Springer, 11–20
- DePoy, D., Abbott, T., Annis, J., et al. 2008, in *Ground-based and Airborne Instrumentation for Astronomy II*, Vol. 7014, SPIE, 190–198
- Dey, A., Schlegel, D. J., Lang, D., et al. 2019, *The Astronomical Journal*, 157, 168
- Flaugher, B., Diehl, H., Honscheid, K., et al. 2015, *The Astronomical Journal*, 150, 150
- Fukugita, M., Ichikawa, T., Gunn, J., et al. 1996, *AJ*, 111, 1748
- Gardner, J. P., Mather, J. C., Clampin, M., Doyon, R., & Wright, G. S. 2009, *Space Science Reviews*, 123, 485

- Gulrajani, I., Ahmed, F., Arjovsky, M., Dumoulin, V., & Courville, A. C. 2017, *Advances in neural information processing systems*, 30
- Hashimoto, Y., Oemler Jr, A., Lin, H., & Tucker, D. L. 1998, *The Astrophysical Journal*, 499, 589
- He, K., Zhang, X., Ren, S., & Sun, J. 2016, in *Proceedings of the IEEE conference on computer vision and pattern recognition*, 770–778
- Holmberg, E. 1958, *Meddelanden fran Lunds Astronomiska Observatorium Serie II*, 136, 1
- Huang, R., Wu, H., & Huang, J. 2024, in *Proceedings of the International Conference on Image Processing, Machine Learning and Pattern Recognition*, 577–582
- Hui, W., Jia, Z. R., Li, H., & Wang, Z. 2022, *Journal of Physics: Conference Series*, 2402, 012009
- Ivezić, Ž., Kahn, S. M., Tyson, J. A., et al. 2019, *ApJ*, 873, 111, doi: [10.3847/1538-4357/ab042c](https://doi.org/10.3847/1538-4357/ab042c)
- Jordon, J., Szpruch, L., Houssiau, F., et al. 2022, arXiv preprint arXiv:2205.03257
- Kingma, D. P. 2014, arXiv preprint arXiv:1412.6980
- Krizhevsky, A. 2014, arXiv preprint arXiv:1404.5997
- Lallo, & Matthew, D. 2012, *Optical Engineering*, 51
- Laureijs, R., Amiaux, J., Arduini, S., et al. 2011, arXiv e-prints, arXiv:1110.3193, doi: [10.48550/arXiv.1110.3193](https://doi.org/10.48550/arXiv.1110.3193)
- Leung, H. W., & Bovy, J. 2019, *Monthly Notices of the Royal Astronomical Society*, 483, 3255
- Lintott, C., Schawinski, K., Bamford, S., et al. 2011, *Monthly Notices of the Royal Astronomical Society*, 410, 166
- Lintott, C. J., Schawinski, K., Slosar, A., et al. 2008, *Monthly Notices of the Royal Astronomical Society*, 389, 1179
- Lotz, J. M., Madau, P., Giavalisco, M., Primack, J., & Ferguson, H. C. 2006, *The Astrophysical Journal*, 636, 592
- LSST Science Collaboration: Abell, P. A., Allison, J., Anderson, S. F., et al. 2009, arXiv e-prints, arXiv:0912.0201, doi: [10.48550/arXiv.0912.0201](https://doi.org/10.48550/arXiv.0912.0201)
- Luo, Z., Zhang, S., Chen, J., et al. 2024, arXiv preprint arXiv:2410.20025
- Maile, K., Wilson, D. G., & Forré, P. 2022, arXiv preprint arXiv:2210.05484
- Odena, A. 2016, arXiv preprint arXiv:1606.01583
- Pandya, S., Patel, P., Blazek, J., et al. 2023, arXiv preprint arXiv:2311.01500
- Panwar, S., Rad, P., Quarles, J., Golob, E., & Huang, Y. 2019, in *2019 IEEE International Conference on Systems, Man and Cybernetics (SMC)*, IEEE, 3943–3948
- Parry, O., Eke, V., & Frenk, C. 2009, *Monthly Notices of the Royal Astronomical Society*, 396, 1972
- Radford, A. 2015, arXiv preprint arXiv:1511.06434
- Roberts, M. S., & Haynes, M. P. 1994, *Annual Review of Astronomy and Astrophysics*, Volume 32, 1994, pp. 115-152., 32, 115
- Rodriguez-Gomez, V., Sales, L. V., Genel, S., et al. 2017, *Monthly Notices of the Royal Astronomical Society*, 467, 3083
- Sandage, A. 1986, *Astronomy and Astrophysics (ISSN 0004-6361)*, vol. 161, no. 1, June 1986, p. 89-101. SNSF-supported research., 161, 89
- Simonyan, K., & Zisserman, A. 2014, arXiv preprint arXiv:1409.1556
- Stein, G., Blaum, J., Harrington, P., Medan, T., & Lukić, Z. 2022, *The Astrophysical Journal*, 932, 107
- Sutskever, I., Jozefowicz, R., Gregor, K., et al. 2015, arXiv preprint arXiv:1511.06440
- Thanh-Tung, H., & Tran, T. 2020, in *2020 international joint conference on neural networks (ijcnn)*, IEEE, 1–10
- Tremblay, J., Prakash, A., Acuna, D., et al. 2018, in *Proceedings of the IEEE conference on computer vision and pattern recognition workshops*, 969–977
- Walmsley, M., Lintott, C., Géron, T., et al. 2022, *Monthly Notices of the Royal Astronomical Society*, 509, 3966
- Willett, K. W., Lintott, C. J., Bamford, S. P., et al. 2013, *Monthly Notices of the Royal Astronomical Society*, 435, 2835
- Yao, Y., Zhang, J., Du, P., & Dong, S. 2024, *Research in Astronomy and Astrophysics*, 24, 035015
- York, D. G., Adelman, J., Anderson, John E., J., et al. 2000, *AJ*, 120, 1579, doi: [10.1086/301513](https://doi.org/10.1086/301513)
- Zeng, S., Zhang, H., Chen, Y., et al. 2023, *Computers and Electronics in Agriculture*, 213, 108226
- Zhan, H. 2021, *Chinese Science Bulletin*, 66, 1290
- Zhang, H. 2017, arXiv preprint arXiv:1710.09412
- Zou, H., Zhou, X., Fan, X., et al. 2019, *The Astrophysical Journal Supplement Series*, 245, 4